

pyPPG: A Python toolbox for comprehensive photoplethysmography signal analysis

Márton Á. Goda¹, Peter H. Charlton² and Joachim A. Behar¹

¹Faculty of Biomedical Engineering, Technion Institute of Technology, Technion-IIT, Haifa, 32000, Israel.

²Department of Public Health and Primary Care, University of Cambridge, Cambridge, CB1 8RN, United Kingdom.

Abstract

Photoplethysmography is a non-invasive optical technique that measures changes in blood volume within tissues. It is commonly and increasingly used for in a variety of research and clinical application to assess vascular dynamics and physiological parameters. Yet, contrary to heart rate variability measures, a field which has seen the development of stable standards and advanced toolboxes and software, no such standards and open tools exist for continuous photoplethysmogram (PPG) analysis. Consequently, the primary objective of this research was to identify, standardize, implement and validate key digital PPG biomarkers. This work describes the creation of a standard Python toolbox, denoted *pyPPG*, for long-term continuous PPG time series analysis recorded using a standard finger-based transmission pulse oximeter. The improved PPG peak detector had an F1-score of 88.19% for the state-of-the-art benchmark when evaluated on 2,054 adult polysomnography recordings totaling over 91 million reference beats. This algorithm outperformed the open-source original Matlab implementation by $\sim 5\%$ when benchmarked on a subset of 100 randomly selected MESA recordings. More than 3,000 fiducial points were manually annotated by two annotators in order to validate the fiducial points detector. The detector consistently demonstrated high performance, with a mean absolute error of less than 10 ms for all fiducial points. Based on these fiducial points, *pyPPG* engineers a set of 74 PPG biomarkers. Studying the PPG time series variability using *pyPPG* can enhance our understanding of the manifestations and etiology of diseases. This toolbox can also be used for biomarker engineering in training data-driven models. *pyPPG* is available on physiozoo.org (upon publication.).

Keywords: photoplethysmography, beat detection, digital biomarkers.

1 Introduction

Photoplethysmography is an optical sensing technique widely used for health and fitness monitoring in clinical and consumer devices [22], such as smartwatches and pulse oximeters. Photoplethysmography was developed in the 1930s [6], and its potential value for assessing cardiovascular health was recognised in the 1940s [34]. It was not until the 1970s that photoplethysmography became widely used as the sensing technology in pulse oximeters [9]. Photoplethysmography-based wearable devices entered the consumer market in the 2010s [24], and are now used by millions of people for unobtrusive health monitoring [55].

The photoplethysmogram (PPG) signal contains a wealth of information on the heart, blood vessels, breathing, and autonomic nervous system [6]. Consequently, much research is focused on extracting physiological information from the PPG [52], including physiological parameters such as blood pressure and breathing rate [18, 54], and disease indicators, such as vascular age and cardiovascular risk markers [22, 25]. The value of photoplethysmography is rapidly increasing: its value for heart rate and oxygen saturation monitoring is well established, its utility for detecting atrial fibrillation has recently been demonstrated [61], and its potential to detect other diseases such as sleep apneas and peripheral arterial disease is being researched [22, 25]. Despite the widespread and increasing use of photoplethysmography, there is a lack of open-source tools for detailed analysis of the PPG. This paper presents *pyPPG*, an open-source, validated Python toolbox for PPG signal analysis.

1.1 The photoplethysmogram (PPG) signal

The PPG signal is an optical measurement of the arterial pulse wave [23], *i.e.*, the wave generated when blood is ejected from the heart, temporarily increasing arterial pressure and causing vessel expansion and contraction [5]. Consequently, the PPG signal is influenced by a range of physiological systems, such as: the heart, including heart rate, heart rhythm, and the nature of ejection [22]; the blood vessels, including vessel stiffness, diameter, and blood pressure [22]; the microvasculature, including peripheral compliance and resistance [22]; the autonomic nervous system which influences heart rate variability [38]; and the respiratory system, which impacts the pulse wave through changes in intrathoracic pressure [19]. Thus, there is potential to extract much physiological information from the PPG signal.

The PPG signal can be acquired using a range of sensors and devices. PPG sensors consist of a light source such as an LED, and a light sensor, such as a photodiode [68]. The light source illuminates a region with vasculature, such as the fingertip, and the light sensor measures how much light is either transmitted through or reflected from the tissue. The amount of light received fluctuates with each heartbeat: usually, the amount of absorbed light increases during systole when blood volume is greatest, and then decreases during diastole when blood volume returns to its initial level [6]. This produces a pulse wave bearing several features, which can be interpreted as physiological biomarkers (see Figure 2) [22]. In pulse oximeters, the PPG is typically acquired in transmission mode using a fingerclip probe [57], while in consumer devices such as smartwatches, fitness trackers, and earbuds (*i.e. hearables*), it is typically acquired reflection mode [24].

1.2 Applications of photoplethysmography

At present, the most common applications of photoplethysmography are for heart rate monitoring in smartwatches [71], and for oxygen saturation monitoring in pulse oximeters [57]. Smartwatches, fitness trackers and hearables are widely used, with an estimated 1.1 billion connected wearable devices world-wide in 2022 [66]. Pulse oximetry is a standard-of-care technique used in a range of clinical settings from intensive care to home monitoring [40, 58]. Recently, the applications of photoplethysmography-based wearables have been expanded to include atrial fibrillation detection [61], blood pressure monitoring [79], and oxygen saturation monitoring [64]. Several additional potential applications of wearable photoplethysmography devices are being researched [72], including sleep staging [44], mental health assessment [15, 50], identifying obstructive sleep apnea [11, 12], and detecting peripheral arterial disease [65]. Each of these applications uses PPG signal analysis to derive physiological information from the PPG.

Photoplethysmography confers several advantages over other physiological monitoring technologies, which has resulted in its widespread adoption. Measurements can be obtained quickly without the need for a trained operator, and photoplethysmography sensors are non-invasive, unobtrusive, and low-cost. It is also a more compact and accessible monitoring modality than other measurements such as electrocardiogram (ECG) and blood pressure measurement. Furthermore, PPG measurements can be obtained without significantly disrupting daily activities, while ECG electrodes for instance may require careful placement and proper skin preparation to ensure accurate readings. However, a key disadvantage is that the PPG signal is highly susceptible to noise, such as in the cases of poor sensor contact or motion [46].

1.3 Standardising PPG signal analysis

A key step in the use of photoplethysmography for health and fitness monitoring is the development of PPG signal analysis algorithms. Such algorithms typically extract either inter-beat-intervals (*e.g.*, for detection of atrial fibrillation) or features of PPG pulse wave shape (*e.g.*, for estimation of blood pressure). However, unlike in other fields such as heart rate variability analysis, there are no standards for PPG signal analysis, and only limited open tools are available. Consequently, standardized and reproducible analysis of PPG signals is lacking. Although there are some open-source PPG toolboxes, they lack validation and are often incomplete (see Table 1).

Despite the extensive research and applications in the field of PPG analysis, there is an urgent need to standardize approaches, terminologies, variables and definitions. Furthermore, there is no comprehensive toolbox available that covers all standard PPG biomarkers. It is important to acknowledge that certain variables may have different terminologies in the scientific literature, but our objective was to unify them to facilitate a broader understanding of PPG biomarkers. To fill this gap, we have developed a standardized nomenclature and toolbox. The assigned names for variables aim to provide insights into their origin, while the definitions ensure accurate interpretation and improved comprehensibility.

1.4 Paper overview

The primary aim of this research was to create a standardized toolbox (*pyPPG*) to analyze long-term finger PPG recordings in real-time. This paper presents standardized definitions for the state-of-the-art PPG fiducial points and biomarkers implemented within the *pyPPG* toolbox. It provides an overview of the steps involved in raw data processing and biomarker engineering, as well as a validation of the fiducial point extraction process (see Figure 1). Additionally, the paper presents performance results and benchmarks them against other publicly available toolboxes.

Table 1 Comparison of open-source PPG signal processing libraries: *pyPPG* (this work), *PPGFeat* [1], *PulseAnalyse* [23], *NeuroKit2* [51], *RRest* [30], *PPGSynth* [70], *PhysioNet Cardiovascular Signal Toolbox (PCST)* [77], *HeartPy* [75, 76], *BioSPPy* [16]

	<i>pyPPG</i>	<i>PPGFeat</i>	<i>PulseAnalyse</i>	<i>NeuroKit2</i>	<i>RRest</i>	<i>PPGSynth</i>	<i>PCST</i>	<i>HeartPy</i>	<i>BioSPPy</i>
<i>Prefiltering</i>	✓	✓	✓	✓	✓	✓	✓	✓	✓
<i>Peak detection</i>	✓	✓	✓	✓	✓	✓	✓	✓	✓
<i>Onset detection</i>	✓	✓	✓	✓	✓	–	✓	–	✓
<i>Other fiducial points</i>	✓	✓	✓	–	–	–	–	–	–
<i>Biomarker engineering</i>	✓	–	✓	–	–	–	–	–	–
<i>Signal quality</i>	✓	–	✓	–	✓	✓	✓	✓	–
<i>Quantitative validation</i>	✓	✓	–	–	–	–	✓	✓	–

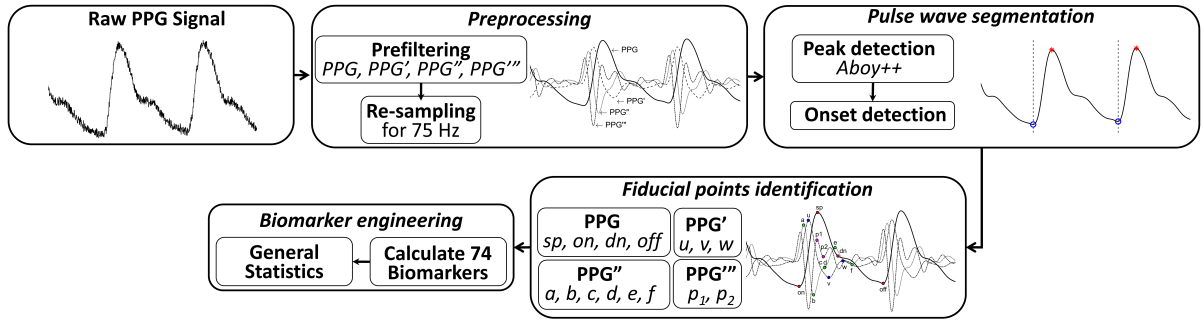


Fig. 1 Flowchart for continuous PPG time series analysis. The analysis comprises several key components, including: Preprocessing, Pulse wave segmentation, Fiducial points identification and Biomarker engineering.

2 Materials and methods

2.1 Databases

Two databases were used to validate the *pyPPG* toolbox. The Multi-Ethnic Study of Atherosclerosis (MESA) database [32, 82] was used to validate our peak detector, and the PPG and Blood Pressure (PPG-BP) database [47] was used to validate the fiducial point detection algorithm. The MESA database consists of polysomnography (PSG) recordings from 2,056 adults aged 54–95 years, with subclinical cardiovascular disease, including 19,998 hours of PPG recordings [26, 63]. Males accounted for 45.5% of the subjects. The database was downloaded from the National Sleep Resource Center [82]. The institutional review board from the Technion-IIT Rapport Faculty of Medicine was obtained under number 62-2019 in order to use the retrospective databases obtained from the open-access sleepdata.org resource for this research. The PSG recordings in MESA were acquired at home, including fingertip PPG signals measured at 256 Hz from the fingertip using Nonin 8000 series pulse oximeters (Nonin Medical Inc., Plymouth, US), alongside simultaneous ECG signals. The PPG-BP dataset contains 657 short (2 s) PPG recordings collected from 219 adult subjects aged 20–89 years with different health statuses (including healthy, hypertensive and diabetic subjects). Males accounted for 48% of the subjects. The data include fingertip PPG signals measured at 1 kHz using a SEP9AF-2 PPG sensor (SMPLUS Company, Korea). Signals were acquired using a 12-bit ADC, and the hardware applied a 0.5–12Hz band-pass filter.

Table 2 Fingertip PPG databases used for the quantitative validation experiments

Database	Number of subjects	Length of recordings	Gender(M:F)	Filtering	Sampling rate	Age
MESA	2056	~10-hour	1:1.2	digital	256 Hz	54-95
PPG-BP	219	2-second	1:1.08	hardware	1 kHz	20-89

2.2 Overview of the *pyPPG* toolbox

The *pyPPG* toolbox is a standardized resource for real-time analysis of long-term finger PPG recordings. The toolbox consists of five main components, as summarized in Figure 1:

1. **Loading a raw PPG signal:** The toolbox can accept various file formats such as *.mat*, *.csv*, *.txt*, or *.edf*. These files should contain raw PPG data along with the corresponding sampling rate.
2. **Preprocessing:** The raw signal is filtered to remove unwanted noise and artifacts. Subsequently, the signal is resampled to a uniform rate of 75 Hz.

3. **Pulse wave segmentation:** The toolbox employs a peak detector to identify the systolic peaks. Based on the peak locations, the toolbox also detects the pulse onsets and offsets, which indicate the start and end of the PPG pulse waves.
4. **Fiducial points identification:** For each pulse wave, the toolbox detects a set of fiducial points.
5. **Biomarker engineering:** Based on the fiducial points, a set of 74 PPG digital biomarkers are engineered.

The *pyPPG* toolbox also provides an optional PPG signal quality index based on the Matlab implementation of the work by Li *et al.* [46].

2.3 Preprocessing

The PPG signal filtering is one of the most essential parts of preprocessing. The human heart rate ranges between 30 and 200 beats per minute [59]. Therefore in PPG signal analysis, it is common to apply bandpass filtering such: 0.5–8 Hz [1], 0.5–10 Hz [37], 0.5–15 Hz [52], 0.5–20 Hz [7, 47], or 0.5–25 Hz [27], to conserve the frequency content of the PPG pulse waves while filtering out lower frequency content (e.g. baseline wander due to respiration) and higher frequency content (e.g. muscle noise or power interference).

We selected a frequency range of 0.5–12 Hz. Whilst fiducial point detection can be simpler with lower low-pass cut-off frequencies such as 8 Hz, the drawback of using lower cut-off frequencies is that they significantly distort the pulse wave shape and reduce the accuracy with which the pulse onset and other fiducial points can be identified. Conversely, cut-off frequencies above 12 Hz can make it more complex to detect fiducial points due to the presence of extra waves in the PPG derivatives. Therefore, during the benchmarking process of other toolboxes for fiducial point detection (see Section 3.2), the 0.5–12 Hz frequency band was employed for filtering purposes. Although the 0.5–12 Hz band is recommended by default for PPG analysis, it is possible for the user to customize the passband filter in the *pyPPG* toolbox.

To meet the above-mentioned requirements, the following zero-phase filters were implemented:

1. **Bandpass filtering between 0.5–12 Hz:** A fourth-order Chebyshev Type II filter was used for the original signal. The 12 Hz low-pass cut-off was used to avoid time-shifting of fiducial points (particularly pulse onset, and dicrotic notch) and to eliminate unwanted high-frequency content from the PPG derivatives. The 0.5 Hz high-pass cut-off was used to minimize baseline wandering whilst retaining content at low heart rates.
2. **20 ms moving average filtering (MAF):** In the case of very noisy signals, some high-frequency content can remain in the band-pass filter signal. For this purpose, a 20 ms standard flat (boxcar or top-hat) MAF with a 22.5 Hz cut-off frequency was applied after the band-pass filtering.
3. **10 ms MAF for the PPG derivatives:** To eliminate the high-frequency content in the PPG derivatives, a 10 ms standard flat (boxcar or top-hat) MAF with 45 Hz cut-off frequency was applied.

It is common for the PPG signal to be sampled at over 100 Hz and up to 1 kHz, as, for example, in the PPG-BP dataset. However, an excessive sampling frequency may not be ideal for long-term data processing due to the computational load. The default behavior of the toolbox is to resample PPG signals at 75 Hz using the Python *resample* function using the Fourier method.

2.4 Pulse wave segmentation

The toolbox identifies individual pulse waves in a PPG signal by identifying systolic peaks (*sp*), and then identifying the pulse onset (*on*) and offset (*off*) on either side of each systolic peak which indicate the start and end of the pulse wave, respectively.

Systolic peak detection

The *sp* is the most important fiducial point of the PPG signal (see Figure 2). It is defined as the point with the highest amplitude between two consecutive pulse onsets (see Fig. 2). The *pyPPG* toolbox uses

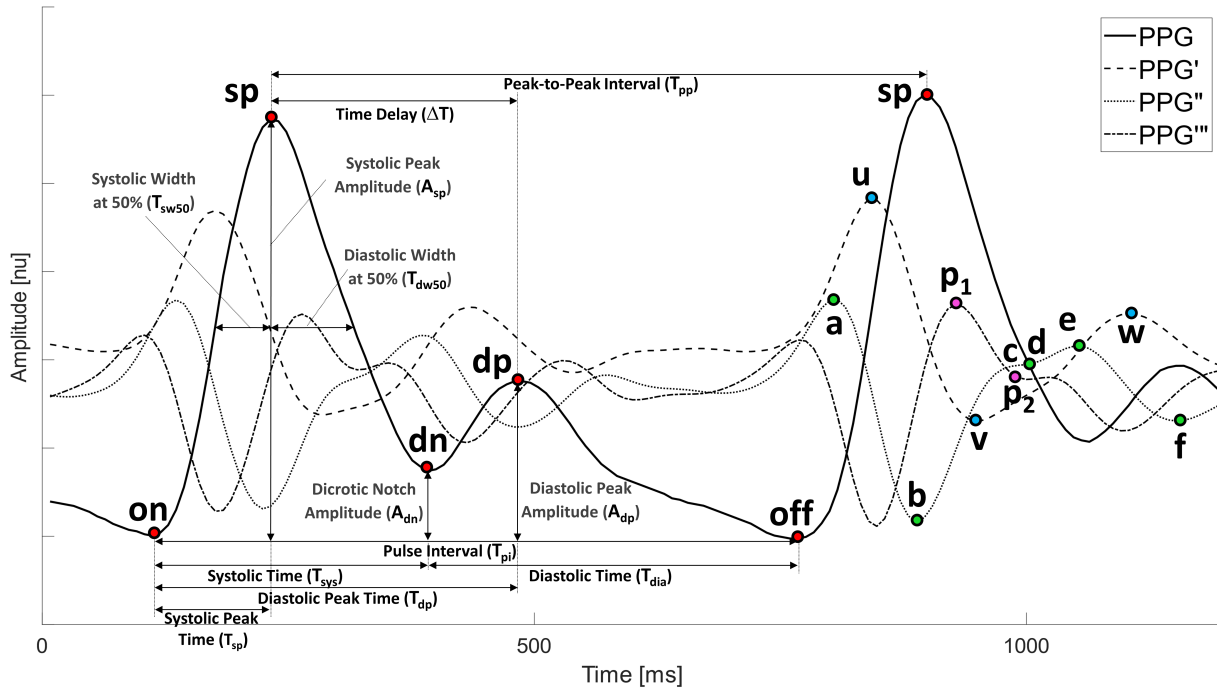


Fig. 2 The fiducial points of the PPG signal include the systolic peak (sp), the pulse onset and offset (on , off), the dicrotic notch (dn), and the diastolic peak (dp). The fiducial points of PPG derivatives are represented by u , v , w , a , b , c , d , e , f , p_1 , p_2 . The biomarkers are calculated based on this set of fiducial points.

Table 3 Definition of PPG fiducial points

FIDUCIAL POINTS		Ref
PPG		
1 on	<i>Pulse onset</i> . The beginning of the systolic upslope, typically, but not necessarily, a minimum point	
2 sp	<i>Systolic peak</i> . The highest amplitude between two consecutive pulse onsets	
3 dn	<i>Dicrotic notch</i> . If a diastolic peak is present, then it is the local minimum preceding the diastolic peak. If there is no diastolic peak, then it is the inflection point between the systolic peak and f-point	
4 dp	<i>Diastolic peak</i> . The first local maximum of the PPG pulse wave after the dicrotic notch and before the 0.8 pulse interval; if no maxima then the first local maximum of PPG' pulse wave after the e-point and before the 0.8 pulse interval.	[69]
5 off	<i>Pulse offset</i> : The local minimum preceding the next pulse wave's systolic upslope	
PPG'		
5 u	The highest amplitude between the pulse onset and systolic peak on PPG'	[8]
6 v	The lowest amplitude between the u-point and diastolic peak on PPG'	[67]
7 w	The first local maximum or inflection point after the dicrotic notch on PPG'	[67]
PPG''		
8 a	The highest amplitude between pulse onset and systolic peak on PPG''	[69]
9 b	The first local minimum after the a-point on PPG''	[69]
10 c	The local maximum with the highest amplitude between the b-point and e-point, or if no local maximum is present then the inflection point on PPG''	[69]
11 d	The local minimum with the lowest amplitude between the c-point and e-point, or if no local minimum is present then the inflection point on PPG''	[69]
12 e	The local maximum with the highest amplitude after the b-point and before the diastolic peak on PPG''	[69]
13 f	The first local minimum after the e-point on PPG''	[69]
PPG'''		
14 p_1	The first local maximum after the b-point on PPG'''	[20]
15 p_2	The last local minimum after the b-point and before the d-point on PPG'''	

an enhanced *sp* detection algorithm to enable real-time analysis of long-term PPG measurements. The algorithm is an enhanced version of the Aboy beat detector [2], which performed either best [42], or amongst the best [21] in recent benchmarking studies of PPG beat detectors. We focused on improving the beat detector's performance and reducing its computational complexity.

The original *Aboy* algorithm utilizes an advanced filtering technique to accurately detect systolic peaks [2]. PPG recordings are segmented into 10-second windows and then filtered using three digital filters. The first filter helps to estimate the heart rate, while the second and third filters are used for peak detection. Two modifications were made to the *Aboy* algorithm [2]. Firstly, to enhance the speed of the previous Matlab implementation [21], the finite impulse response (FIR) filter was replaced by a zero-phase fifth-order Chebyshev Type II infinite impulse response (IIR) filter, which applied the same cut-off frequencies as the original *Aboy* peak detector. Secondly, the enhanced algorithm includes adaptive heart rate estimation to handle strong baseline wandering and rapid amplitude fluctuations [39]. The resulting modified peak detector is denoted *Aboy++*.

Pulse onset detection

The *on* corresponds to the beginning of the pulse wave and the beginning of the systolic upslope (see Figure 2 and Table 3). This systolic upslope is caused by increasing arterial pressure during systole [3]. *on* is typically a minimum point, but not necessarily. *pyPPG* includes a novel *on* detection algorithm. Previously, *on* has been identified as the minimum value between two successive detected *sp* [36, 74], or identified using the slope sum function approach [33, 56]. However, during long-term measurements there can be multiple local minima between successive *sp*, particularly in a noisy PPG signal. We define the *on* as the initiation of the systolic upslope, which is usually a minimum point, although not always. We used a simple yet accurate approach to detect the *on* as the first maximum preceding the p_1 -point on the PPG". *off* is equivalent to the *on* on the next pulse wave.

2.5 Fiducial points identification

Dicrotic notch detection

The dicrotic notch (*dn*) plays an important role as a fiducial point in the analysis of PPG signals, holding immense potential for various applications such as heart disease detection [41] and arterial stiffness assessment [3]. Its significance stems from its association with the duration of systole, which is known to be affected by heart disease. Additionally, the appearance of the diastolic wave following the *dn* allows for the evaluation of arterial stiffness, with the hypothesis that the presence of the *dn* is influenced by the arterial stiffness. However, it should be noted that the visibility of the *dn* diminishes progressively with age, making it typically no longer discernible in elderly subjects [25].

None of the existing definitions of *dn* are entirely satisfactory. Typically, the *dn* is easily recognizable when a distinct local minimum exists between the *sp* and the *dp* (see Figure 2). Yet, in many cases, the *dp* is not clearly visible, rendering it difficult to accurately identify the *dn*. Dawber *et al.* [31] categorized different classes of *dn*, which are illustrated in Figure 3. Another morphological approach for *dn* identification involves locating it at the time of zero-crossing of the PPG" between the *d* and *e* points [17]. However, debate regarding the precise location for defining the *dn* is ongoing. For instance, situations may arise where the local minimum of the *dn* is visible, but the occurrence of the *d* and *e* points precedes the zero-crossing point, as depicted in Figure 2.

Fiducial points of PPG derivatives

Additional fiducial points were defined on the PPG derivatives (PPG', PPG" and PPG''') as depicted in Figure 2 [25, 67]. The fiducial point detection algorithms in *pyPPG* are based on standardized, morphological definitions (see Table 3). Consequently, these points do not necessarily correspond to points with consistent physiological interpretations. On the PPG' signal, the maximum point of the systolic slope

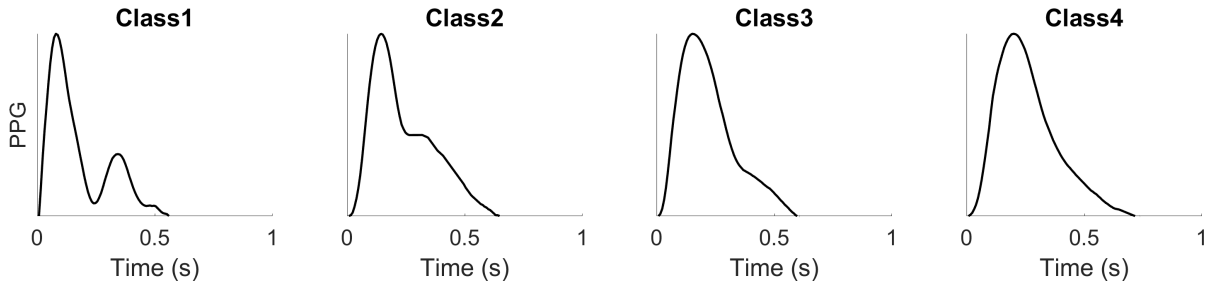


Fig. 3 The dicrotic notch (dn) is considered visible when there is a local minimum between the sp and dp . However, the dp is not always clearly visible. The dn can be classified into four classes: Class 1, in which the dn is with an incisura, Class 2, in which there is a horizontal line at the dn , Class 3, in which there is a change in gradient on the downslope, or and Class 4, in which there is no clear evidence of the dn . The figure was adapted from Charlton *et al.* [25].

is denoted as the u -point, while the minimum point is referred to as the v -point. The u -point has been used to assess arterial stiffness [78]. On the PPG^{''} signal, six further fiducial points are defined. Among these, four points (a , b , c , and d) are typically observed during the systolic phase (see Figure 2). As the diastolic phase begins, the e -point becomes visible, followed by the appearance of the f -point [67]. Points a to e have been used to assess vascular ageing [69], and the d -point has been identified as a predictor of cardiovascular mortality. On the PPG^{'''} signal, p_1 represents the early systolic component of the PPG pulse wave, while p_2 corresponds to the late systolic component [69]. p_1 and p_2 are used to calculate the augmentation index, which has been found to be elevated in atherosclerotic and diabetic subjects [14, 62].

2.6 Biomarker engineering

The *pyPPG* toolbox includes a comprehensive collection of 74 standard PPG morphological biomarkers which are calculated from the timings and amplitudes of the fiducial points (see Tables 4, 5, 6, 7). The biomarkers were categorized into four groups: (1) PPG Signal - biomarkers that are based on the location of the fiducial points of the PPG signal; (2) Signal Ratios - biomarkers that are based on ratios of the fiducial points of the PPG signal; (3) PPG Derivatives - biomarkers that are based on the location of the fiducial points of the PPG derivatives; and (4) Derivatives Ratios - biomarkers that are based on ratios of the fiducial points of the PPG derivatives.

For a given window consisting of a set of beats, *pyPPG* provides the following nine general statistics for each biomarker (see Supplementary Table S2, S3, S4, S5): signal duration; average (AVG); median (MED); standard deviation (STD); lower and upper quartiles (Q1, Q3); inter-quartile range (IQR); Skewness (SKW, indicating a lack of symmetry in the distribution; Kurtosis (KUR, indicating the pointedness of a peak in the distribution curve); and the average difference between the mean and each data value (MAD).

2.7 Validation

Systolic peak detection

The performance and computational complexity of the enhanced sp detection algorithm, *Aboy++*, were evaluated. Performance was assessed in comparison to reference ECG-derived beats using the F_1 -score, which is a commonly used statistic for evaluating the performance of such algorithms. The F_1 -score is particularly suitable for this purpose because it effectively combines multiple fractional measures by utilizing a harmonic mean between the sensitivity and positive predictive value. F_1 -scores are reported as median (MED) and quartiles (Q1, Q3). The performance and computational complexity of *Aboy++* were compared against the implementation of *Aboy* provided by Charlton *et al.* [21]. Due to the high computational needs of *Aboy*, the two algorithms were compared on a subset of MESA consisting of 100 recordings (1,173 hours) of PPG. *Aboy++* was then assessed on the entire MESA database, with the exception of two recordings which did not have an ECG reference signal. Thus 2,054 PPG recordings were

Table 4 Biomarkers derived from the PPG signal categorized into intervals, amplitudes, and areas

PPG SIGNAL			Ref
1	T_{pi}	Pulse interval, the time between the pulse onset and pulse offset	[27]
2	T_{pp}	Peak-to-peak interval, the time between two consecutive systolic peaks	[45]
3	T_{sys}	Systolic time, the time between the pulse onset and dicrotic notch	[4]
4	T_{dia}	Diastolic time, the time between the dicrotic notch and pulse offset	[4]
5	T_{sp}	Systolic peak time, the time between the pulse onset and systolic peak	[8]
6	T_{dp}	Diastolic peak time, the time between the pulse onset and diastolic peak	[28]
7	ΔT	Time delay, the time between the systolic peak and diastolic peak	[28]
8	T_{swx}	Systolic width, the width at x% of the systolic peak amplitude between the pulse onset and systolic peak	[45]
9	T_{dwx}	Diastolic width, the width at x% of the systolic peak amplitude between the systolic peak and pulse offset	[45]
10	T_{pwx}	Pulse width, the sum of the systolic width and diastolic width at x%	[45]
11	A_{sp}	Systolic peak amplitude, the difference in amplitude between the pulse onset and systolic peak	[29]
12	A_{dn}	Dicrotic notch amplitude, the difference in amplitude between the pulse onset and dicrotic notch	[35]
13	A_{dp}	Diastolic peak amplitude, the difference in amplitude between the pulse onset and diastolic peak	[35]
14	A_{off}	Pulse onset amplitude, the difference in amplitude between the pulse onset and pulse offset	
15	AUC_{pi}	Area under pulse interval curve, the area under the pulse wave between pulse onset and pulse offset	[35]
16	AUC_{sys}	Area under systolic curve, the area under the pulse wave between the pulse onset and dicrotic notch	[4]
17	AUC_{dia}	Area under diastolic curve, the area under the pulse wave between the dicrotic notch and pulse offset	[4]

Table 5 Biomarkers derived from the signal ratios categorized into intervals, amplitudes, areas, and combinations thereof

SIGNAL RATIOS			Ref
1	IPR	Instantaneous pulse rate, $60/T_{pi}$	[49]
2	T_{sys}/T_{dia}	Ratio of the systolic time vs. the diastolic time	[4]
3	T_{pwx}/T_{pi}	Ratio of the pulse width at x% of the systolic peak amplitude vs. the pulse interval	[27]
4	T_{pwx}/T_{ps}	Ratio of the pulse width at x% of the systolic peak amplitude vs. the systolic peak time	[27]
5	T_{dwx}/T_{swx}	Ratio of the diastolic width vs. the systolic width at x% width	[45]
6	T_{sp}/T_{pi}	Ratio of the systolic peak time vs. the pulse interval	
7	A_{sp}/A_{off}	Ratio of the systolic peak amplitude vs. the pulse offset amplitude	
8	A_{dp}/A_{sp}	Reflection index, ratio of the diastolic peak amplitude vs. the systolic peak amplitude	[28]
9	IPA	Inflection point area, ratio of the area under diastolic curve vs. the area under systolic curve	[80]
10	T_{sp}/A_{sp}	Ratio of the systolic peak time vs. the systolic peak amplitude	[48]
11	$A_{sp}/\Delta T$	Stiffness index, ratio of the systolic peak amplitude vs. the time delay	[53]
12	$A_{sp}/(T_{pi}-T_{sp})$	Ratio of the systolic peak amplitude vs. the difference between the pulse interval and systolic peak time	[27]

Table 6 Biomarkers derived from the PPG derivatives

		PPG DERIVATIVES	Ref
1		T_u	ms
2		T_v	[67]
3		T_w	[67]
4		T_a	[67]
5		T_b	[67]
6		T_c	[67]
7		T_d	[67]
8	Intervals	T_e	[67]
9		T_f	[67]
10		T_{b-c}	[20]
11		T_{b-d}	[20]
12		T_{p_1}	[67]
13		T_{p_2}	[67]
14		T_{p_1-dp}	[60]
15		T_{p_2-dp}	[60]

Table 7 Biomarkers derived from the derivatives ratios categorized into intervals, amplitudes, areas, and combinations of these

		DERIVATIVES RATIOS	Ref
1		T_u/T_{pi}	[27]
2		T_v/T_{pi}	[27]
3		T_w/T_{pi}	[27]
4		T_a/T_{pi}	[27]
5	Intervals	T_b/T_{pi}	[27]
6		T_c/T_{pi}	[27]
7		T_d/T_{pi}	[27]
8		T_e/T_{pi}	[27]
9		T_f/T_{pi}	[27]
10		$(T_u - T_a)/T_{pi}$	[27]
11		$(T_v - T_b)/T_{pi}$	[27]
12		A_u/A_{sp}	[8]
13		A_v/A_u	[69]
14		A_w/A_u	[69]
15		A_b/A_a	[69]
16		A_c/A_a	[69]
17		A_d/A_a	[69]
18		A_e/A_a	[69]
19		A_f/A_a	[69]
20	Amplitudes	A_{p_2}/A_{p_1}	[60]
21		$(A_c - A_b)/A_a$	[4]
22		$(A_d - A_b)/A_a$	[4]
23		AGI	[69]
24		AGI_{mod}	[73]
25		AGI_{inf}	[10]
26		AI	[69]
27		RI_{p_1}	[60]
28		RI_{p_2}	[60]
29	Combined	SC	[81]
30		$IPAD$	[4]

included, consisting of more than 19,000 hours of continuous PPG signals and over 91 million reference beats. The median recording length was 10 hours, with a 2.5-hour interquartile range (IQR). The 10-hour-long recordings were divided into 10-minute segments. Segments were excluded if they did not contain a minimum of 300 ECG reference beats or if the extracted biomarkers could not be successfully evaluated. A key step in this assessment was to synchronise the timings of ECG-derived beats and PPG systolic peaks. This was achieved by forecasting the PPG *sp* by extracting electrocardiogram (ECG) peaks from the PSG recordings as a reference signal similar to the work of Kotzen *et al.* [43]. The evaluation metric was based on the alignment of the ECG-R-wave and PPG *sp*. The methods for performance assessment are elaborated in more detail in our previous work [39, 43].

Fiducial point detection

The fiducial point detection algorithm was validated by comparison against the manual annotations of the PPG-BP [47] database. The data were manually annotated by two annotators (MAG and PHC) following the definitions in Table 3. An annotation tool was adapted from the open source *RRest toolbox* for this purpose [19]. If an annotator could not confidently identify a fiducial point then they did not annotate it. After both annotators independently annotated the prefiltered signal, the time difference between the two annotators annotations was calculated. If the time discrepancy was >10 ms, then the annotators discussed the case and either: (i) agreed on a location; or (ii) excluded the fiducial point (i.e. the annotators were not confident of its location). The final reference annotations were determined as the average of the annotations provided by the two annotators. In the PPG-BP database, each subject has three recordings. The first complete, high-quality pulse wave was selected for each subject. In total, more than 3,000 fiducial points from 219 patients were manually annotated by the two annotators. The PPG signals were filtered within the frequency band of 0.5-12 Hz during the manual annotation and benchmarking of the toolboxes (see Section 3.2). The Inter-rater reliability of annotations is presented in Table S1.

To assess the performance of the fiducial point detection algorithm, *pyPPG* was benchmarked against two publicly available PPG toolboxes capable of detecting fiducial points (*PulseAnalyse* [23] and *PPGFeat* [1]). Both benchmarked toolboxes were implemented in Matlab. Performance was assessed using the mean absolute error (MAE) and the standard deviation of the absolute errors (STD) of the fiducial point detections in comparison to the reference. Bland-Altman plots [13] with the limits of agreement (1.96STD, indicating 95% of errors) are also included.

3 Results

3.1 Systolic peak detection

The improved *sp* detector, *Aboy++*, outperformed the original *Aboy* implementation when benchmarked on a subset of 100 randomly selected MESA recordings. The F_1 -score of *Aboy++* was ~5% greater than that of *Aboy*. In addition, the computational time of *Aboy++* was over 57 times faster than that of *Aboy*. Specifically, the median peak detection time for 1-hour-long segments was 114.24 seconds for *Aboy*, compared to 1.98 seconds for *Aboy++*. When evaluated on the 2,054 recordings of the MESA dataset, *Aboy++* obtained an F_1 -score of 88.19% (81.73–92.71).

3.2 Fiducial points detection

The results for the benchmarking of *pyPPG* against other PPG toolboxes (*PulseAnalyse* and *PPGFeat*) are presented in Table 8. A total of 219 distinct pulse waves were employed for the benchmarking process. The MAEs were <10 ms with *pyPPG* for all fiducial points. *pyPPG* outperformed the other toolboxes: The MAEs for *pyPPG* were less than half of those for *PPGFeat* for all fiducial points, and less than those for *PulseAnalyse* for all except two fiducial points. In comparison to the other toolboxes, *pyPPG* showed particular improvements in the detection of dn , p_1 , and p_2 . In addition, *pyPPG* was able to detect

Table 8 Benchmark of PPG toolboxes for fiducial points detection. The mean (and standard deviation) of the absolute errors are reported for each fiducial in ms.

Fiducial Point	<i>on</i>	<i>dn</i>	<i>u</i>	<i>v</i>	<i>w</i>	<i>a</i>	<i>b</i>	<i>c</i>	<i>d</i>	<i>e</i>	<i>f</i>	p_1	p_2
<i>pyPPG (this work)</i>	8(13)	9(15)	1(1)	1(1)	3(14)	1(1)	1(1)	3(6)	5(9)	3(9)	3(11)	1(1)	1(2)
<i>PulseAnalyse [23]</i>	8(25)	26(23)	2(1)	-	-	1(1)	2(1)	9(26)	9(27)	3(18)	5(21)	39(36)	30(42)
<i>PPGFeat [1]</i>	50(139)	40(56)	9(16)	13(38)	48(99)	16(32)	10(21)	19(36)	23(45)	28(59)	39(77)	-	-

fiducial points which were not detected by *PulseAnalyse* (*v* and *w*) or *PPGFeat* (p_1 , p_2). A standard Bland-Altman plot was generated to present the differences between the manual annotations and the *pyPPG* fiducial points detection (see Figure 3.2).

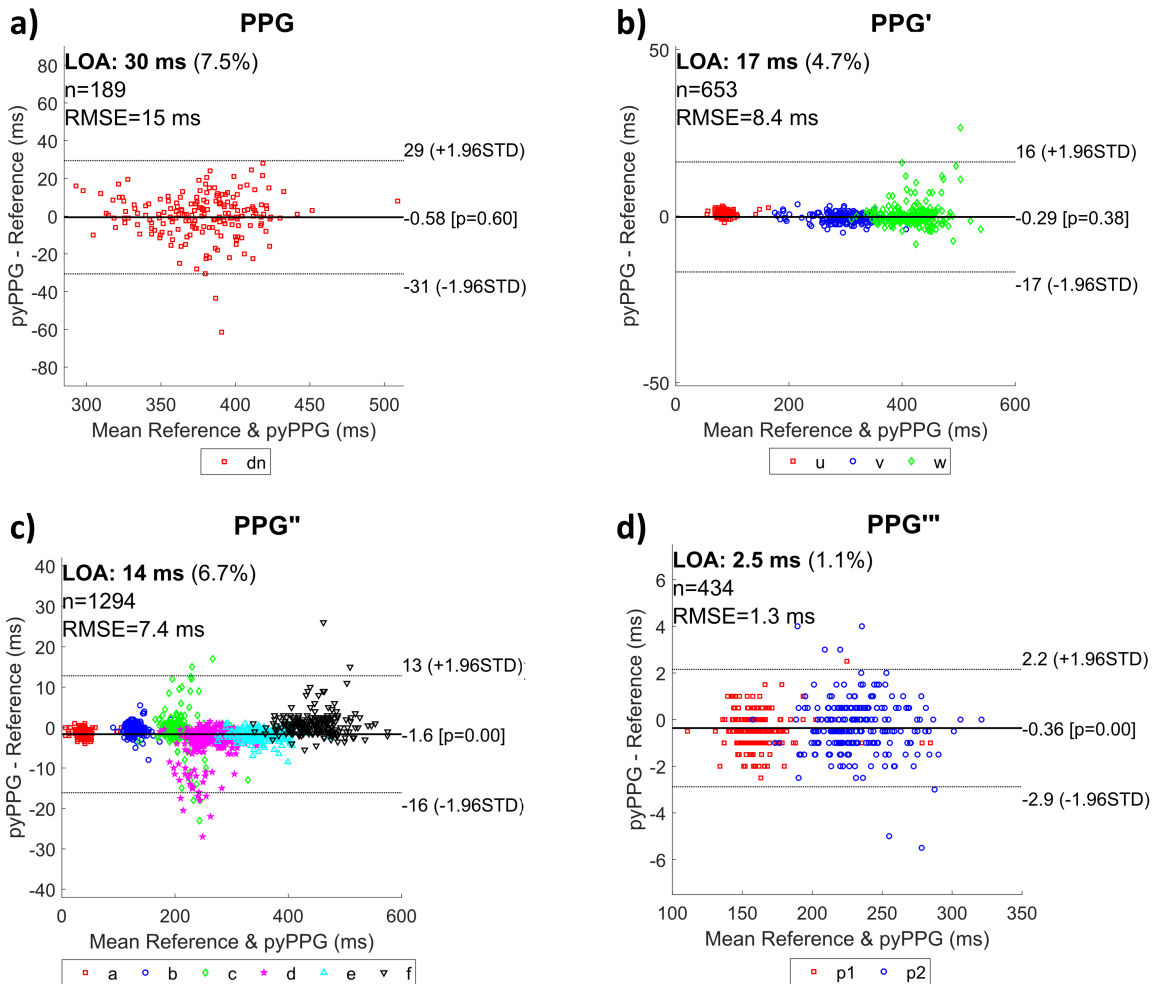


Fig. 4 Bland-Altman plot comparing the detected fiducial points and manual annotations at 99% percentile of the data, with the reference pulse onset serving as the starting point. The panels (a) to (d) depict the results of the PPG signal and its derivatives. LOA: limits of agreement, n: number of fiducial points, RMSE: root mean squared error, STD: standard deviation of the differences.

3.3 *pyPPG* and PhysioZoo PPG

The resulting systolic peak detection and fiducial points detection algorithms are package into an open source Python library denoted *pyPPG*. In addition, a user-friendly interface is also implemented in the [PhysioZoo Software](#). In order to ensure that *pyPPG* could process a large dataset without technical issues, we run it over the full MESA database and reported standard statistics for all biomarkers (see Supplementary Table [S2](#), [S3](#), [S4](#), [S5](#)). (The library and software will be placed online following publication.)

4 Discussion

This work is expected to contribute significantly to the scientific field of computerized cardiology, leading to a better understanding of the PPG signal. Firstly, it standardized the definition of PPG fiducial points and biomarkers. The second major contribution consists in the implementation and quantitative validation of a fiducial point detector. The peak detection algorithm in the *pyPPG* toolbox was validated on 19,000 hours of continuous PPG data, encompassing more than 91 million reference beats. It performed with an 88.18% F_1 -score while processing a 1-hour segment in 1.98 seconds. When evaluated on 3,000 manually annotated fiducial points *pyPPG* had a low MAE and consistently outperformed two other open toolboxes.

The third key contribution pertains to the implementation in *pyPPG* of 74 physiological PPG. The toolbox is made open-source, making it the only comprehensive and validated Python library that is publicly accessible. A user-friendly interface is also implemented in the [PhysioZoo Software](#) software. This interface enables data visualization, exploration and quantitative analysis of a PPG recording. By offering this novel solution, researchers and clinicians are empowered with a valuable resource for comprehensive and reproducible PPG analysis. Finally, the manual annotations of the 219 recordings, including more than 3,000 fiducial points are made open access to ensure reproducibility of the results and to enable further investigations and advancements in the field of PPG analysis.

This research has limitations. The performance of the peak detection algorithms were only performed on sleep data from atherosclerosis patients (see Supplementary Table [S2](#), [S3](#), [S4](#), [S5](#)). Therefore the evaluation of Aboy++ on additional databases would be very beneficial. Another limitation of the work is the focus on the analysis of PPG measured using standard clinical oximeter. Adapting the toolbox to incorporate PPG sources like earlobe PPG or smartwatches will also be of interest, particularly given the widespread use of the later. The program has another limitation related to the controversial nature of morphological and physiological characteristics of fiducial points (see Supplementary Figure ??). Hence, creating a standardized toolbox presented a significant challenge.

In conclusion, this work provides a standards and advanced toolbox for the analysis of PPG. Studying the PPG time series variability using *pyPPG* can enhance our understanding of the manifestations and etiology of diseases. This toolbox can also be used for biomarker engineering in training data-driven models.

5 Code Availability

The source code used and the annotations of the fiducial points in this research are available at physiozoo.com.

6 Acknowledgments

MAG and JAB acknowledge the Estate of Zofia (Sophie) Fridman and funding from the Israel Innovation Authority. PHC acknowledges funding from the British Heart Foundation (grant FS/20/20/34626).

The Multi-Ethnic Study of Atherosclerosis (MESA) Sleep Ancillary study was funded by NIH-NHLBI Association of Sleep Disorders with Cardiovascular Health Across Ethnic Groups (RO1 HL098433).

MESA is supported by NHLBI funded contracts HHSN268201500003I, N01-HC-95159, N01-HC-95160, N01-HC-95161, N01-HC-95162, N01-HC-95163, N01-HC-95164, N01-HC-95165, N01-HC-95166, N01-HC-95167, N01-HC-95168 and N01-HC-95169 from the National Heart, Lung, and Blood Institute, and by cooperative agreements UL1-TR-000040, UL1-TR-001079, and UL1-TR-001420 funded by NCATS. The National Sleep Research Resource was supported by the National Heart, Lung, and Blood Institute (R24 HL114473, 75N92019R002).

References

- [1] Saad Abdullah, Abdelakram Hafid, Mia Folke, Maria Lindén, and Annica Kristoffersson. Ppgfeat: a novel matlab toolbox for extracting ppg fiducial points. *Frontiers in Bioengineering and Biotechnology*, 11, 2023.
- [2] Mateo Aboy, James McNames, Tran Thong, Daniel Tsunami, Miles S. Ellenby, and Brahm Goldstein. An automatic beat detection algorithm for pressure signals. *IEEE Transactions on Biomedical Engineering*, 52:1662–1670, 10 2005.
- [3] Paul S. Addison. Slope transit time (stt): A pulse transit time proxy requiring only a single signal fiducial point. *IEEE Transactions on Biomedical Engineering*, 63:2441–2444, 11 2016.
- [4] Jae Mok Ahn. New aging index using signal features of both photoplethysmograms and acceleration plethysmograms. *Healthcare informatics research*, 23(1):53–59, 2017.
- [5] Jordi Alastruey, Peter H Charlton, Vasiliki Bikia, Birute Paliakaitė, Bernhard Hametner, Rosa Maria Bruno, Marijn P Mulder, Samuel Vennin, Senol Piskin, Ashraf W Khir, et al. Arterial pulse wave modelling and analysis for vascular age studies: a review from vascagenet. *American Journal of Physiology-Heart and Circulatory Physiology*, 2023.
- [6] John Allen. Photoplethysmography and its application in clinical physiological measurement. *Physiological measurement*, 28(3):R1, 2007.
- [7] John Allen and Alan Murray. Similarity in bilateral photoplethysmographic peripheral pulse wave characteristics at the ears, thumbs and toes. *Physiological measurement*, 21(3):369, 2000.
- [8] Stephen R Alty, Sandrine C Millasseau, PJ Chowienzcyc, and Andreas Jakobsson. Cardiovascular disease prediction using support vector machines. In *2003 46th Midwest Symposium on Circuits and Systems*, volume 1, pages 376–379. IEEE, 2003.
- [9] Takuo Aoyagi. Pulse oximetry: its invention, theory, and future. *Journal of anesthesia*, 17:259–266, 2003.
- [10] Hyun Jae Baek, Jung Soo Kim, Yun Sung Kim, Haet Bit Lee, and Kwang Suk Park. Second derivative of photoplethysmography for estimating vascular aging. In *2007 6th International Special Topic Conference on Information Technology Applications in Biomedicine*, pages 70–72. IEEE, 2007.
- [11] Joachim Behar, Aoife Roebuck, Mohammed Shahid, Jonathan Daly, Andre Hallack, Niclas Palmius, John Stradling, and Gari D Clifford. Sleepap: an automated obstructive sleep apnoea screening application for smartphones. *IEEE journal of biomedical and health informatics*, 19(1):325–331, 2014.
- [12] Joachim A Behar, Niclas Palmius, Qiao Li, Silverio Garbuio, Fabiòla PG Rizzatti, Lia Bittencourt, Sergio Tufik, and Gari D Clifford. Feasibility of single channel oximetry for mass screening of obstructive sleep apnea. *EClinicalMedicine*, 11:81–88, 2019.

- [13] J Martin Bland and DouglasG Altman. Statistical methods for assessing agreement between two methods of clinical measurement. *The lancet*, 327(8476):307–310, 1986.
- [14] Luiz A Bortolotto, Jacques Blacher, Takeshi Kondo, Kenji Takazawa, and Michel E Safar. Assessment of vascular aging and atherosclerosis in hypertensive subjects: second derivative of photoplethysmogram versus pulse wave velocity. *American journal of hypertension*, 13(2):165–171, 2000.
- [15] Ayse S Cakmak, Erick A Perez Alday, Giulia Da Poian, Ali Bahrami Rad, Thomas J Metzler, Thomas C Neylan, Stacey L House, Francesca L Beaudoin, Xinming An, Jennifer S Stevens, et al. Classification and prediction of post-trauma outcomes related to ptsd using circadian rhythm changes measured via wrist-worn research watch in a large longitudinal cohort. *IEEE journal of biomedical and health informatics*, 25(8):2866–2876, 2021.
- [16] Carlos Carreiras, Ana Priscila Alves, André Lourenço, Filipe Canento, Hugo Silva, Ana Fred, et al. Biosppy: Biosignal processing in python. *Accessed on*, 3(28):2018, 2015.
- [17] Abhishek Chakraborty, Deboleena Sadhukhan, and Madhuchhanda Mitra. Accurate detection of dicrotic notch from ppg signal for telemonitoring applications. *International Journal of Biomedical Engineering and Technology*, 37(2):121–137, 2021.
- [18] Peter H Charlton, Drew A Birrenkott, Timothy Bonnici, Marco AF Pimentel, Alistair EW Johnson, Jordi Alastruey, Lionel Tarassenko, Peter J Watkinson, Richard Beale, and David A Clifton. Breathing rate estimation from the electrocardiogram and photoplethysmogram: A review. *IEEE reviews in biomedical engineering*, 11:2–20, 2017.
- [19] Peter H Charlton, Timothy Bonnici, Lionel Tarassenko, Jordi Alastruey, David A Clifton, Richard Beale, and Peter J Watkinson. Extraction of respiratory signals from the electrocardiogram and photoplethysmogram: technical and physiological determinants. *Physiological Measurement*, 38(5):669, 2017.
- [20] Peter H Charlton, Patrick Celka, Bushra Farukh, Phil Chowienczyk, and Jordi Alastruey. Assessing mental stress from the photoplethysmogram: a numerical study. *Physiological measurement*, 39(5):054001, 2018.
- [21] Peter H Charlton, Kevin Kotzen, Elisa Mejía-Mejía, Philip J Aston, Karthik Budidha, Jonathan Mant, Callum Pettit, Joachim A Behar, and Panicos A Kyriacou. Detecting beats in the photoplethysmogram: benchmarking open-source algorithms. *Physiological Measurement*, 43(8):085007, 2022.
- [22] Peter H Charlton, Panicos A Kyriacou, Jonathan Mant, Vaidotas Marozas, Phil Chowienczyk, and Jordi Alastruey. Wearable photoplethysmography for cardiovascular monitoring. *Proceedings of the IEEE*, 110(3):355–381, 2022.
- [23] Peter H Charlton, Jorge Mariscal Harana, Samuel Vennin, Ye Li, Phil Chowienczyk, and Jordi Alastruey. Modeling arterial pulse waves in healthy aging: a database for in silico evaluation of hemodynamics and pulse wave indexes. *American Journal of Physiology-Heart and Circulatory Physiology*, 317(5):H1062–H1085, 2019.
- [24] Peter H Charlton and Vaidotas Marozas. Wearable photoplethysmography devices. In *Photoplethysmography*, pages 401–439. Elsevier, 2022.

- [25] Peter H Charlton, Birutė Paliakaitė, Kristjan Pilt, Martin Bachler, Serena Zanelli, Daniel Kulin, John Allen, Magid Hallab, Elisabetta Bianchini, Christopher C Mayer, et al. Assessing hemodynamics from the photoplethysmogram to gain insights into vascular age: A review from vasagenet. *American Journal of Physiology-Heart and Circulatory Physiology*, 322(4):H493–H522, 2022.
- [26] Xiaoli Chen, Rui Wang, Phyllis Zee, Pamela L Lutsey, Sogol Javaheri, Carmela Alcantara, Chandra L Jackson, Michelle A Williams, and Susan Redline. Racial/ethnic differences in sleep disturbances: the multi-ethnic study of atherosclerosis (mesa). *Sleep*, 38(6):877–888, 2015.
- [27] Moajjem Hossain Chowdhury, Md Nazmul Islam Shuzan, Muhammad E.H. Chowdhury, Zaid B. Mahbub, M. Monir Uddin, Amith Khandakar, and Mamun Bin Ibne Reaz. Estimating blood pressure from the photoplethysmogram signal and demographic features using machine learning techniques. *Sensors (Switzerland)*, 20, 6 2020.
- [28] Philip J Chowienczyk, Ronan P Kelly, Helen MacCallum, Sandrine C Millasseau, Tomas LG Anderson, Raymond G Gosling, James M Ritter, and Erik E Ånggård. Photoplethysmographic assessment of pulse wave reflection: blunted response to endothelium-dependent beta2-adrenergic vasodilation in type ii diabetes mellitus. *Journal of the American College of Cardiology*, 34(7):2007–2014, 1999.
- [29] Chern Pin Chua and Conor Heneghan. Continuous blood pressure monitoring using ecg and finger photoplethysmogram. In *2006 International Conference of the IEEE Engineering in Medicine and Biology Society*, pages 5117–5120. IEEE, 2006.
- [30] MIT Critical Data, Peter H Charlton, Mauricio Villarroel, and Francisco Salguiero. Waveform analysis to estimate respiratory rate. *Secondary Analysis of Electronic Health Records*, pages 377–390, 2016.
- [31] Thomas R Dawber, H Emerson THomas Jr, and Patricia M McNamara. Characteristics of the dicrotic notch of the arterial pulse wave in coronary heart disease. *Angiology*, 24(4):244–255, 1973.
- [32] Dennis A Dean, Ary L Goldberger, Remo Mueller, Matthew Kim, Michael Rueschman, Daniel Mobley, Satya S Sahoo, Catherine P Jayapandian, Licong Cui, Michael G Morrical, et al. Scaling up scientific discovery in sleep medicine: the national sleep research resource. *Sleep*, 39(5):1151–1164, 2016.
- [33] Anagha Vishwas Deshmane. *False arrhythmia alarm suppression using ECG, ABP, and photoplethysmogram*. PhD thesis, Massachusetts Institute of Technology, 2009.
- [34] John B Dillon and Alrick B Hertzman. The form of the volume pulse in the finger pad in health, arteriosclerosis, and hypertension. *American Heart Journal*, 21(2):172–190, 1941.
- [35] Kefeng Duan, Zhiliang Qian, Mohamed Atef, and Guoxing Wang. A feature exploration methodology for learning based cuffless blood pressure measurement using photoplethysmography. In *2016 38th Annual international conference of the IEEE engineering in medicine and biology society (EMBC)*, pages 6385–6388. IEEE, 2016.
- [36] Umar Farooq, Dae-Geun Jang, Jang-Ho Park, and Seung-Hun Park. Ppg delineator for real-time ubiquitous applications. In *2010 Annual International Conference of the IEEE Engineering in Medicine and Biology*, pages 4582–4585, 2010.
- [37] Eoin Finnegan, Shaun Davidson, Mirae Harford, Peter Watkinson, Lionel Tarassenko, and Mauricio Villarroel. Features from the photoplethysmogram and the electrocardiogram for estimating changes in blood pressure. *Scientific Reports*, 13(1):986, 2023.

- [38] Eduardo Gil, Michele Orini, Raquel Bailon, José María Vergara, Luca Mainardi, and Pablo Laguna. Photoplethysmography pulse rate variability as a surrogate measurement of heart rate variability during non-stationary conditions. *Physiological measurement*, 31(9):1271, 2010.
- [39] Marton A. Goda, Peter H. Charlton, and Joachim A. Behar. Robust peak detection for photoplethysmography signal analysis. In *50th Computing in Cardiology conference in Atlanta, Georgia, USA on 1st - 4th October 2023 (accepted)*. IEEE.
- [40] Trisha Greenhalgh, Matthew Knight, Matt Inada-Kim, Naomi J Fulop, Jonathan Leach, and Cecilia Vindrola-Padros. Remote management of covid-19 using home pulse oximetry and virtual ward support. *bmj*, 372, 2021.
- [41] WB Gu, CCY Poon, and YT Zhang. A novel parameter from ppg dicrotic notch for estimation of systolic blood pressure using pulse transit time. In *2008 5th International Summer School and Symposium on Medical Devices and Biosensors*, pages 86–88. IEEE, 2008.
- [42] Kevin Kotzen. *Sleep Architecture and Fragmentation Estimation From Photoplethysmography Using Feature Engineering and Deep Learning*, (Master's thesis, Faculty of Biomedical Engineering, Technion, Israel Institute of Technology, Haifa, Israel). Retrieved from <https://graduate.technion.ac.il/en/advisor-en-21666/>. Technion - Israel Institute of Technology, 2022.
- [43] Kevin Kotzen, Peter H Charlton, Amir Landesberg, and Joachim A Behar. Benchmarking photoplethysmography peak detection algorithms using the electrocardiogram signal as a reference; benchmarking photoplethysmography peak detection algorithms using the electrocardiogram signal as a reference. *2021 Computing in Cardiology (CinC)*, 48, 2021.
- [44] Kevin Kotzen, Peter H Charlton, Sharon Salabi, Lea Amar, Amir Landesberg, and Joachim A Behar. Sleepppg-net: a deep learning algorithm for robust sleep staging from continuous photoplethysmography. *IEEE Journal of Biomedical and Health Informatics*, 2022.
- [45] Yuriy Kurylyak, Francesco Lamonaca, and Domenico Grimaldi. A neural network-based method for continuous blood pressure estimation from a ppg signal. In *2013 IEEE International instrumentation and measurement technology conference (I2MTC)*, pages 280–283. IEEE, 2013.
- [46] Qiao Li and Gari D Clifford. Dynamic time warping and machine learning for signal quality assessment of pulsatile signals. *Physiological measurement*, 33(9):1491, 2012.
- [47] Yongbo Liang, Zhencheng Chen, Guiyong Liu, and Mohamed Elgendi. A new, short-recorded photoplethysmogram dataset for blood pressure monitoring in china. *Scientific data*, 5(1):1–7, 2018.
- [48] Binbin Liu, Zhe Zhang, Xiaohui Di, Xiaoni Wang, Lin Xie, Wenjun Xie, and Jianbao Zhang. The assessment of autonomic nervous system activity based on photoplethysmography in healthy young men. *Frontiers in Physiology*, 12:733264, 2021.
- [49] Markus Lueken, Xiaowei Feng, Boudewijn Venema, Berno JE Misgeld, and Steffen Leonhardt. Photoplethysmography-based in-ear sensor system for identification of increased stress arousal in everyday life. In *2017 IEEE 14th International Conference on Wearable and Implantable Body Sensor Networks (BSN)*, pages 83–86. IEEE, 2017.
- [50] Lynnette Nathalie Lyzwinski, Mohamed Elgendi, and Carlo Menon. The use of photoplethysmography in the assessment of mental health: Scoping review. *JMIR Mental Health*, 10:e40163, 2023.

- [51] Dominique Makowski, Tam Pham, Zen J Lau, Jan C Brammer, François Lespinasse, Hung Pham, Christopher Schölzel, and SH Annabel Chen. Neurokit2: A python toolbox for neurophysiological signal processing. *Behavior research methods*, pages 1–8, 2021.
- [52] Elisa Mejia-Mejia, John Allen, Karthik Budidha, Chadi El-Hajj, Panicos A Kyriacou, and Peter H Charlton. Photoplethysmography signal processing and synthesis. In *Photoplethysmography*, pages 69–146. Elsevier, 2022.
- [53] Sandrine C Millasseau, RP Kelly, JM Ritter, and PJ Chowienczyk. Determination of age-related increases in large artery stiffness by digital pulse contour analysis. *Clinical science*, 103(4):371–377, 2002.
- [54] Ramakrishna Mukkamala, George S Stergiou, and Alberto P Avolio. Cuffless blood pressure measurement. *Annual Review of Biomedical Engineering*, 24:203–230, 2022.
- [55] Aravind Natarajan, Alexandros Pantelopoulos, Hulya Emir-Farinas, and Pradeep Natarajan. Heart rate variability with photoplethysmography in 8 million individuals: a cross-sectional study. *The Lancet Digital Health*, 2(12):e650–e657, 2020.
- [56] Shamim Nemati, Mohammad M. Ghassemi, Vaidehi Ambai, Nino Isakadze, Oleksiy Levantsevych, Amit Shah, and Gari D. Clifford. Monitoring and detecting atrial fibrillation using wearable technology. In *2016 38th Annual International Conference of the IEEE Engineering in Medicine and Biology Society (EMBC)*, pages 3394–3397, 2016.
- [57] Meir Nitzan, Itamar Nitzan, and Yoel Arieli. The various oximetric techniques used for the evaluation of blood oxygenation. *Sensors*, 20(17):4844, 2020.
- [58] Rafael Ortega, Christopher J. Hansen, Kelly Elterman, and Albert Woo. Pulse Oximetry. *New England Journal of Medicine*, 364(16):e33, April 2011.
- [59] Birutė Paliakaitė, Andrius Petrėnas, Andrius Sološenko, and Vaidotas Marozas. Photoplethysmogram modeling of extreme bradycardia and ventricular tachycardia. In *XV Mediterranean Conference on Medical and Biological Engineering and Computing–MEDICON 2019: Proceedings of MEDICON 2019, September 26-28, 2019, Coimbra, Portugal*, pages 1165–1174. Springer, 2020.
- [60] Mikko Peltokangas, Anca A Telembeci, Jarmo Verho, Ville M Mattila, Pekka Ronsi, Antti Vehkaoja, Jukka Lekkala, and Niku Oksala. Parameters extracted from arterial pulse waves as markers of atherosclerotic changes: performance and repeatability. *IEEE journal of biomedical and health informatics*, 22(3):750–757, 2017.
- [61] Marco V Perez, Kenneth W Mahaffey, Haley Hedlin, John S Rumsfeld, Ariadna Garcia, Todd Ferris, Vidhya Balasubramanian, Andrea M Russo, Amol Rajmane, Lauren Cheung, et al. Large-scale assessment of a smartwatch to identify atrial fibrillation. *New England Journal of Medicine*, 381(20):1909–1917, 2019.
- [62] K Pilt, K Meigas, R Ferenets, K Temitski, and M Viigimaa. Photoplethysmographic signal waveform index for detection of increased arterial stiffness. *Physiological measurement*, 35(10):2027, 2014.
- [63] Mantas Rinkevičius, Peter H Charlton, Raquel Bailón, and Vaidotas Marozas. Influence of photoplethysmogram signal quality on pulse arrival time during polysomnography. *Sensors*, 23(4):2220, 2023.

- [64] Carmen Spaccarotella, Alberto Polimeni, Cinzia Mancuso, Girolamo Pelaia, Giovanni Esposito, and Ciro Indolfi. Assessment of non-invasive measurements of oxygen saturation and heart rate with an apple smartwatch: comparison with a standard pulse oximeter. *Journal of clinical medicine*, 11(6):1467, 2022.
- [65] Gerard Stansby, Andrew J Sims, Lesley Wilson, Tom AW Beale, James Wightman, Ina Guri, Scott Wilkes, Shona Haining, John Allen, and NOTEPAD Study Team. Prospective assessment of the diagnostic accuracy of multi-site photoplethysmography pulse measurements for diagnosis of peripheral artery disease in primary care. *Angiology*, page 00033197221121614, 2022.
- [66] Statista. Global connected wearable devices 2019-2022, June 2023.
- [67] Mohd Zubir Suboh, Rosmina Jaafar, Nazrul Anuar Nayan, Noor Hasmiza Harun, and Mohd Shawal Faizal Mohamad. Analysis on four derivative waveforms of photoplethysmogram (ppg) for fiducial points detection. *Frontiers in Public Health*, 2022.
- [68] Yu Sun and Nitish Thakor. Photoplethysmography revisited: from contact to noncontact, from point to imaging. *IEEE transactions on biomedical engineering*, 63(3):463–477, 2015.
- [69] Kenji Takazawa, Nobuhiro Tanaka, Masami Fujita, Osamu Matsuoka, Tokuyu Saiki, Masaru Aikawa, Sinobu Tamura, and Chiharu Ibukiyama. Assessment of vasoactive agents and vascular aging by the second derivative of photoplethysmogram waveform. *Hypertension*, 32(2):365–370, 1998.
- [70] Qunfeng Tang, Zhencheng Chen, John Allen, Aymen Alian, Carlo Menon, Rabab Ward, and Mohamed Elgendi. Ppgsynth: An innovative toolbox for synthesizing regular and irregular photoplethysmography waveforms. *Frontiers in Medicine*, 7:597774, 2020.
- [71] Andriy Temko. Accurate heart rate monitoring during physical exercises using ppg. *IEEE Transactions on Biomedical Engineering*, 64(9):2016–2024, 2017.
- [72] Peter H. Charlton *et al.* The 2023 wearable photoplethysmography roadmap. *Physiological Measurement*, [in press], 2023.
- [73] Takahisa Ushiroyama, Yoshinaga Kajimoto, Kou Sakuma, and Minoru Ueki. Assessment of chilly sensation in japanese women with laser doppler fluxmetry and acceleration plethysmogram with respect to peripheral circulation. *Bull Osaka Med Coll*, 51(2):76–84, 2005.
- [74] Simhadri Vadrevu and M. Sabarimalai Manikandan. A robust pulse onset and peak detection method for automated ppg signal analysis system. *IEEE Transactions on Instrumentation and Measurement*, 68(3):807–817, 2019.
- [75] Paul van Gent, Haneen Farah, Nicole van Nes, and Bart van AreM. Analysing noisy driver physiology real-time using off-the-shelf sensors: Heart rate analysis software from the taking the fast lane project. *Journal of Open Research Software*, 7(1), 2019.
- [76] Paul Van Gent, Haneen Farah, Nicole Van Nes, and Bart Van AreM. Heartpy: A novel heart rate algorithm for the analysis of noisy signals. *Transportation research part F: traffic psychology and behaviour*, 66:368–378, 2019.
- [77] Adriana N Vest, Giulia Da Poian, Qiao Li, Chengyu Liu, Shamim Nemati, Amit J Shah, and Gari D Clifford. An open source benchmarked toolbox for cardiovascular waveform and interval analysis. *Physiological measurement*, 39(10):105004, 2018.

- [78] Emma von Wowern, Gerd Östling, Peter M Nilsson, and Per Olofsson. Digital photoplethysmography for assessment of arterial stiffness: repeatability and comparison with applanation tonometry. *PLoS one*, 10(8):e0135659, 2015.
- [79] Anna Vybornova, Erietta Polychronopoulou, Arlène Wurzner-Ghajarzadeh, Sibylle Fallet, Josep Sola, and Gregoire Wuerzner. Blood pressure from the optical aktiia bracelet: a 1-month validation study using an extended iso81060-2 protocol adapted for a cuffless wrist device. *Blood pressure monitoring*, 26(4):305, 2021.
- [80] L Wang, Emma Pickwell-MacPherson, YP Liang, and Yuan Ting Zhang. Noninvasive cardiac output estimation using a novel photoplethysmogram index. In *2009 annual international conference of the IEEE engineering in medicine and biology society*, pages 1746–1749. IEEE, 2009.
- [81] Ching Chuan Wei. Developing an effective arterial stiffness monitoring system using the spring constant method and photoplethysmography. *IEEE Transactions on Biomedical Engineering*, 60:151–154, 2013.
- [82] Guo-Qiang Zhang, Licong Cui, Remo Mueller, Shiqiang Tao, Matthew Kim, Michael Rueschman, Sara Mariani, Daniel Mobley, and Susan Redline. The National Sleep Research Resource: towards a sleep data commons. *Journal of the American Medical Informatics Association*, 25(10):1351–1358, 05 2018.

7 Supplementary Material

Table S1 Inter-annotator differences for fiducial points

Fiducial Point	<i>sp</i>	<i>on</i>	<i>dn</i>	<i>u</i>	<i>v</i>	<i>w</i>	<i>a</i>	<i>b</i>	<i>c</i>	<i>d</i>	<i>e</i>	<i>f</i>	<i>p</i> ₁	<i>p</i> ₂
MAE (STD) ms	3(4)	2(3)	3(5)	1(1)	2(2)	2(3)	2(2)	3(2)	3(3)	2(3)	3(2)	2(3)	1(1)	1(2)

The mean and standard deviation of the absolute errors (MAE and STD respectively) are reported for each fiducial in ms.

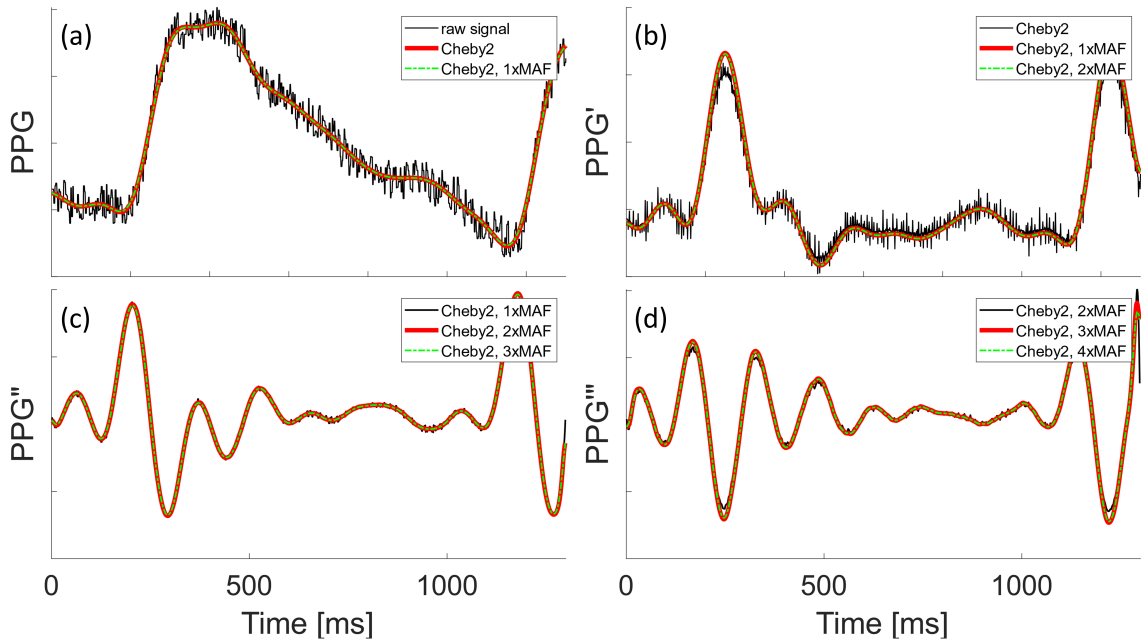


Fig. S1 Prefiltering of the PPG, PPG', PPG'', and PPG''' signals. In panel (a), the raw PPG signal is represented by the black curve, while the red curve represents the application of a fourth-order Chebyshev Type II filter (Cheby2). In panels (a) to (d), the green dashed curve represents the filtered version of the red curve obtained through moving average filtering (MAF). Panels (b) to (d) display the PPG', PPG'', and PPG''' signals, respectively. The black curve depicts the derivatives of the green curve from the preceding panel. Likewise, the red curve corresponds to the derivative of the green curve shown in the previous panel.

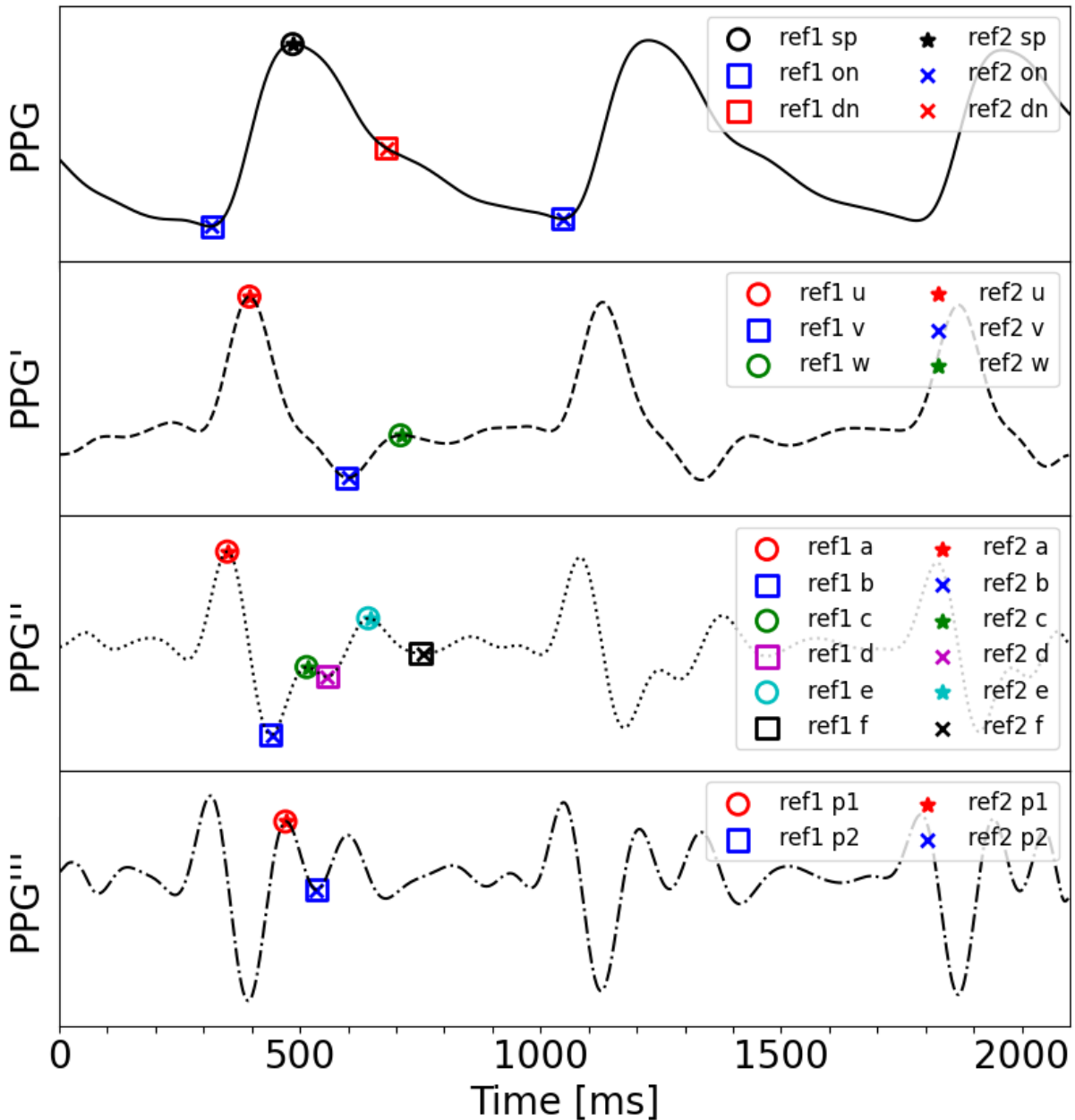


Fig. S2 Comparison of fiducial point annotations. The first manual reference annotation is represented by empty circles and squares, while the crosses and stars indicate the mark of the second annotator. The black lines illustrate the PPG signal and its derivatives. More than 3000 fiducial points were manually annotated in 219 different PPG waves by two annotators on the PPG-BP dataset to validate the implemented fiducial points detector

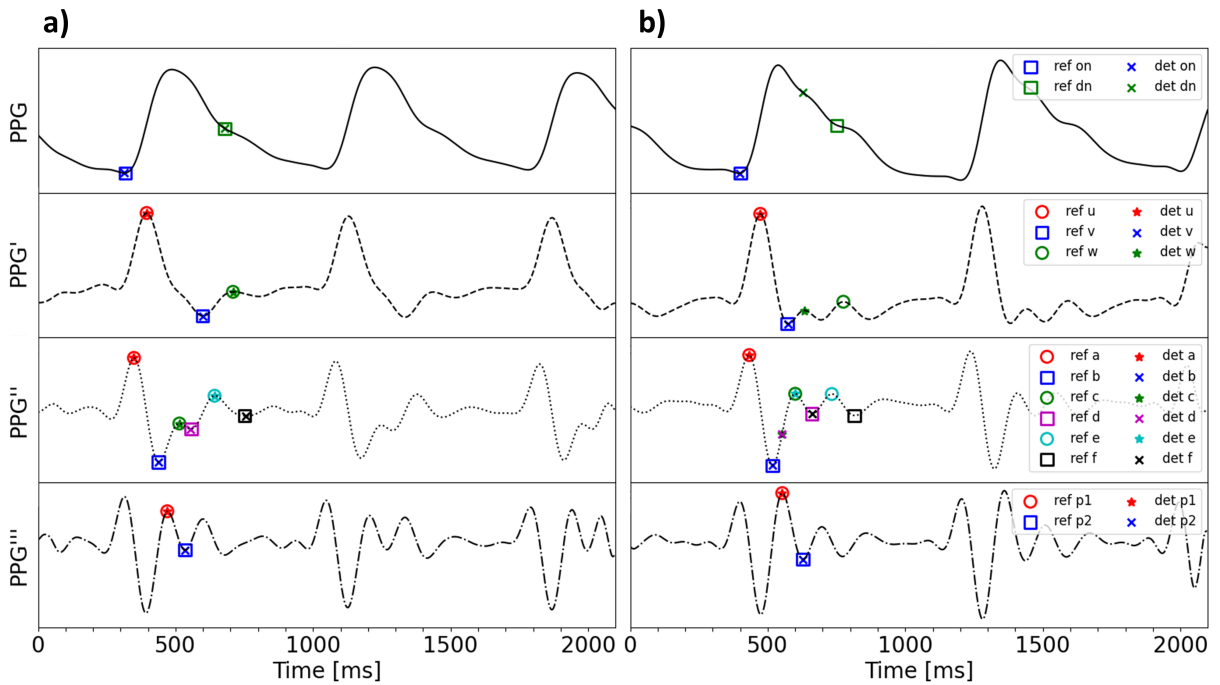


Fig. S3 A comparison between high and low-quality PPG signals. In panel (a), a high-quality signal is illustrated, where all fiducial points are clearly detectable. However, in panel (b), the fiducial point detections are inaccurate due to the low quality of the signal. The reference fiducial points are represented by empty circles and squares, while the detected points are indicated by crosses and stars.

Table S2 Summary statistics for biomarkers of PPG signal from the MESA database for 2,054 PPG recordings

BIOMARKER	AVG	MED	STD	PPG SIGNAL			SKW	KUR	MAD	Unit
				Q1	Q3	IQR				
T_{pi}	0.85	0.83	0.15	0.79	0.88	0.10	3.19	29.44	0.09	s
T_{pp}	0.85	0.83	0.14	0.79	0.88	0.09	2.71	24.63	0.08	s
T_{sys}	0.38	0.36	0.07	0.34	0.39	0.05	4.08	38.56	0.04	s
T_{dia}	0.47	0.47	0.13	0.41	0.51	0.10	1.89	20.18	0.08	s
T_{sp}	0.21	0.20	0.05	0.18	0.22	0.04	4.50	46.99	0.03	s
T_{dp}	0.38	0.36	0.07	0.34	0.39	0.05	4.08	38.56	0.04	s
ΔT	0.17	0.16	0.05	0.14	0.19	0.05	2.12	14.02	0.03	s
T_{sw10}	0.16	0.16	0.04	0.14	0.18	0.04	2.96	27.86	0.03	s
T_{sw25}	0.14	0.14	0.04	0.12	0.16	0.03	2.68	26.06	0.02	s
T_{sw33}	0.13	0.13	0.04	0.11	0.15	0.03	2.57	25.51	0.02	s
T_{sw50}	0.11	0.11	0.03	0.10	0.13	0.03	2.32	23.75	0.02	s
T_{sw66}	0.10	0.09	0.03	0.08	0.11	0.03	2.12	22.20	0.02	s
T_{sw75}	0.08	0.08	0.03	0.07	0.10	0.03	2.11	22.22	0.02	s
T_{sw90}	0.06	0.05	0.02	0.04	0.06	0.02	2.45	23.71	0.01	s
T_{dw10}	0.50	0.50	0.13	0.44	0.55	0.11	1.39	16.16	0.08	s
T_{dw25}	0.38	0.37	0.12	0.33	0.42	0.09	2.04	18.59	0.08	s
T_{dw33}	0.33	0.32	0.12	0.27	0.36	0.09	2.30	19.30	0.07	s
T_{dw50}	0.23	0.21	0.10	0.18	0.25	0.07	3.21	24.36	0.06	s
T_{dw66}	0.16	0.14	0.09	0.12	0.17	0.05	4.51	38.24	0.05	s
T_{dw75}	0.13	0.11	0.08	0.09	0.13	0.04	5.18	47.43	0.04	s
T_{dw90}	0.07	0.06	0.07	0.05	0.07	0.02	6.14	63.89	0.03	s
T_{pw10}	0.67	0.66	0.14	0.61	0.72	0.11	1.60	18.13	0.09	s
T_{pw25}	0.52	0.51	0.13	0.47	0.56	0.10	2.05	19.56	0.08	s
T_{pw33}	0.46	0.45	0.12	0.40	0.50	0.10	2.22	19.76	0.08	s
T_{pw50}	0.35	0.33	0.11	0.29	0.38	0.08	2.86	22.45	0.07	s
T_{pw66}	0.25	0.24	0.10	0.21	0.27	0.06	4.00	34.20	0.05	s
T_{pw75}	0.21	0.19	0.09	0.17	0.22	0.04	4.58	42.41	0.05	s
T_{pw90}	0.13	0.12	0.08	0.10	0.14	0.04	5.18	53.15	0.04	s
A_{sp}	0.20	0.18	0.12	0.14	0.22	0.07	3.50	34.29	0.06	nu
A_{dn}	0.10	0.10	0.10	0.07	0.13	0.06	1.01	34.45	0.05	nu
A_{dp}	0.09	0.08	0.09	0.06	0.11	0.05	2.31	34.98	0.05	nu
A_{off}	0.00	0.00	0.07	-0.01	0.01	0.02	1.03	40.12	0.03	nu
AUC_{pi}	9.50	9.71	97.74	8.64	10.48	1.83	-0.27	162.91	13.21	nu
AUC_{sys}	4.37	4.33	23.77	3.76	4.97	1.20	-0.24	148.02	3.49	nu
AUC_{dia}	5.13	5.21	74.42	4.06	6.18	2.12	-0.18	158.93	10.21	nu

Average (AVG); median (MED); standard deviation (STD); lower and upper quartiles (Q1, Q3); inter-quartile range (IQR); Skewness (SKW, indicating a lack of symmetry in the distribution); Kurtosis (KUR, indicating the pointedness of a peak in the distribution curve); and the average difference between the mean and each data value (MAD).

Table S3 Summary statistics for biomarkers of signal ratios from the MESA database for 2,054 PPG recordings

BIOMARKER	AVG	MED	STD	SIGNAL RATIOS			SKW	KUR	MAD	Unit
				Q1	Q3	IQR				
<i>IPR</i>	73.45	73.33	9.87	69.33	77.50	8.16	0.41	12.57	6.53	%
T_{sys}/T_{dia}	91.33	81.22	39.32	71.41	98.41	27.00	393.22	2923.76	24.38	%
T_{pw25}/T_{pi}	62.00	62.75	10.52	57.08	68.00	10.91	-85.54	610.45	7.62	%
T_{pw50}/T_{pi}	40.87	39.97	9.85	35.34	45.27	9.93	78.04	627.29	7.09	%
T_{pw75}/T_{pi}	24.74	23.54	7.83	21.02	26.51	5.49	247.90	1915.65	4.88	%
T_{pw25}/T_{sp}	266.17	260.62	76.87	226.93	294.03	67.10	174.35	1698.59	50.18	%
T_{pw50}/T_{sp}	174.02	165.78	61.20	144.75	189.08	44.33	289.07	2596.04	36.91	%
T_{pw75}/T_{sp}	105.68	98.58	47.91	86.73	111.63	24.90	435.03	4669.79	24.71	%
T_{dw10}/T_{sw10}	336.94	323.76	132.82	271.42	380.80	109.38	250.74	2289.27	82.14	%
T_{dw25}/T_{sw25}	298.33	277.70	148.79	229.72	333.07	103.35	355.27	3273.42	84.17	%
T_{dw33}/T_{sw33}	277.89	252.94	155.82	207.23	308.78	101.55	400.58	3716.32	85.66	%
T_{dw50}/T_{sw50}	230.45	195.56	176.10	159.28	246.41	87.13	519.26	5062.43	86.84	%
T_{dw66}/T_{sw66}	197.33	154.47	212.89	123.35	199.78	76.43	634.82	6779.45	91.84	%
T_{dw75}/T_{sw75}	187.13	137.75	244.73	108.57	182.58	74.01	685.40	7569.23	99.48	%
T_{dw90}/T_{sw90}	185.76	114.54	373.62	90.54	154.42	63.88	800.79	9758.14	132.09	%
T_{sp}/T_{pi}	24.80	24.11	5.44	21.71	26.99	5.28	195.60	1503.32	3.80	%
A_{sp}/A_{off}	-251.50	-225.29	5093.80	-265.99	-190.83	75.16	-79.27	15171.47	673.97	%
A_{dp}/A_{sp}	50.65	47.32	306.54	37.37	56.42	19.05	-132.42	8856.26	54.04	%
<i>IPA</i>	1.35	1.24	19.00	0.95	1.50	0.55	0.21	146.18	2.53	nu
T_{sp}/A_{sp}	2.59	1.89	41.34	1.41	2.63	1.22	5.04	118.11	6.17	nu
$A_{sp}/\Delta T$	1.32	1.13	1.06	0.87	1.48	0.61	4.26	43.19	0.54	nu
$A_{sp}/(T_{pi}-T_{sp})$	0.32	0.28	0.21	0.23	0.36	0.13	3.78	36.18	0.11	nu

Average (AVG); median (MED); standard deviation (STD); lower and upper quartiles (Q1, Q3); inter-quartile range (IQR); Skewness (SKW, indicating a lack of symmetry in the distribution); Kurtosis (KUR, indicating the pointedness of a peak in the distribution curve); and the average difference between the mean and each data value (MAD).

Table S4 Summary statistics for biomarkers of PPG derivative from the MESA database for 2,054 PPG recordings

BIOMARKER	AVG	MED	STD	PPG DERIVATIVES			SKW	KUR	MAD	Unit
				Q1	Q3	IQR				
T_u	0.11	0.08	0.11	0.06	0.11	0.05	6.21	62.13	0.06	s
T_v	0.38	0.33	0.15	0.29	0.42	0.13	3.24	20.96	0.11	s
T_w	0.42	0.37	0.16	0.32	0.47	0.14	2.80	15.51	0.11	s
T_a	0.06	0.04	0.08	0.03	0.07	0.04	6.05	60.85	0.04	s
T_b	0.11	0.09	0.08	0.08	0.12	0.04	5.33	50.57	0.05	s
T_c	0.15	0.13	0.09	0.11	0.17	0.06	4.04	32.39	0.05	s
T_d	0.22	0.21	0.11	0.16	0.27	0.11	2.02	11.56	0.07	s
T_e	0.35	0.34	0.11	0.30	0.39	0.09	1.38	13.26	0.07	s
T_f	0.38	0.37	0.11	0.33	0.43	0.10	1.33	11.52	0.08	s
T_{b-c}	0.04	0.03	0.02	0.02	0.04	0.02	0.87	1.69	0.01	s
T_{b-d}	0.11	0.10	0.07	0.06	0.15	0.09	1.28	5.24	0.05	s
T_{p1}	0.13	0.11	0.08	0.09	0.14	0.05	4.92	44.11	0.05	s
T_{p2}	0.21	0.19	0.10	0.14	0.25	0.11	2.31	13.10	0.07	s
T_{p1-dp}	0.25	0.25	0.08	0.22	0.28	0.06	-0.41	19.47	0.05	s
T_{p2-dp}	0.17	0.17	0.10	0.11	0.23	0.11	-0.57	7.90	0.07	s

Average (AVG); median (MED); standard deviation (STD); lower and upper quartiles (Q1, Q3); inter-quartile range (IQR); Skewness (SKW, indicating a lack of symmetry in the distribution); Kurtosis (KUR, indicating the pointedness of a peak in the distribution curve); and the average difference between the mean and each data value (MAD).

Table S5 Summary statistics for biomarkers of PPG derivative from the MESA database for 2,054 PPG recordings

BIOMARKER	AVG	MED	DERIVATIVES RATIOS				SKW	KUR	MAD	Unit
			STD	Q1	Q3	IQR				
T_u/T_{pi}	11.18	8.44	11.57	7.32	9.95	2.63	498.54	2700.88	5.23	%
T_v/T_{pi}	49.82	41.88	19.96	34.71	63.47	28.76	82.65	-12.92	16.85	%
T_w/T_{pi}	54.02	45.93	20.01	38.84	67.60	28.76	80.94	-12.58	16.85	%
T_a/T_{pi}	5.80	4.07	7.96	2.59	5.52	2.94	547.31	3988.16	3.88	%
T_b/T_{pi}	11.42	10.28	8.04	8.44	11.72	3.28	539.86	4105.76	3.88	%
T_c/T_{pi}	15.07	14.05	8.46	11.35	16.66	5.31	469.69	3478.37	4.59	%
T_d/T_{pi}	25.59	23.16	12.71	16.50	32.05	15.55	134.11	393.65	9.83	%
T_e/T_{pi}	38.89	40.33	13.68	31.87	47.13	15.26	-3.42	169.26	10.24	%
T_f/T_{pi}	43.02	44.63	13.63	35.81	51.29	15.48	-2.06	162.95	10.28	%
$(T_u - T_a)/T_{pi}$	5.33	3.53	8.88	2.96	6.07	3.12	550.25	4378.08	3.95	%
$(T_v - T_b)/T_{pi}$	38.33	30.90	19.59	24.38	52.20	27.82	69.31	-26.89	16.40	%
A_u/A_{sp}	11.44	11.29	10.85	9.85	12.91	3.06	-342.27	19223.85	3.01	%
A_v/A_u	-56.53	-50.35	31.53	-65.01	-40.28	24.74	-581.35	6066.96	17.48	%
A_w/A_u	8.39	6.60	21.72	-5.48	21.43	26.91	-23.67	268.64	16.59	%
A_b/A_a	-67.51	-71.60	62.78	-96.23	-41.67	54.56	-366.50	5557.12	39.35	%
A_c/A_a	8.73	6.21	42.85	-14.34	30.65	44.99	151.81	1769.14	30.31	%
A_d/A_a	-75.06	-67.10	68.71	-94.36	-48.42	45.95	-515.47	7369.81	36.15	%
A_e/A_a	76.99	66.61	88.58	46.56	90.78	44.22	916.64	14471.11	32.28	%
A_f/A_a	-56.11	-48.07	68.51	-70.78	-25.96	44.82	-576.39	6746.56	33.40	%
A_{p2}/A_{p1}	29.51	127.29	1310.75	24.64	204.19	179.55	-845.24	12641.48	370.00	%
$(A_c - A_b)/A_a$	76.24	69.03	75.93	30.69	107.35	76.65	559.28	7767.55	46.26	%
$(A_d - A_b)/A_a$	-7.55	6.35	69.52	-33.05	34.80	67.84	-152.71	442.67	50.05	%
AGI	-78.17	-69.51	112.94	-113.36	-28.24	85.11	-706.72	11560.28	57.14	%
AGI_{mod}	-1.18	-9.10	66.72	-44.11	42.13	86.23	45.44	152.19	52.43	%
AGI_{inf}	-144.50	-130.56	132.13	-172.72	-99.70	73.01	-831.10	13837.36	54.63	%
AI	42.33	38.33	84.63	17.14	57.40	40.26	924.79	13287.84	36.73	%
RI_{p1}	132.42	111.38	2657.66	83.44	154.65	71.21	325.91	17081.63	504.55	%
RI_{p2}	132.42	111.38	2657.66	83.44	154.65	71.21	325.91	17081.63	504.55	%
SC	0.00	0.00	0.00	0.00	0.00	0.00	-16.01	271.47	0.00	nu
IPAD	1.93	0.43	29.07	-0.01	0.79	0.80	10.28	235.07	3.64	nu

Average (AVG); median (MED); standard deviation (STD); lower and upper quartiles (Q1, Q3); inter-quartile range (IQR); Skewness (SKW, indicating a lack of symmetry in the distribution); Kurtosis (KUR, indicating the pointedness of a peak in the distribution curve); and the average difference between the mean and each data value (MAD).